Journal of Hazardous Materials 199–200 (2012) 255–261

Contents lists available at SciVerse ScienceDirect

Journal of Hazardous Materials

journal homepage: www.elsevier.com/locate/jhazmat

# Experimental study on ozone photolytic and photocatalytic degradation of $H_2S$ using continuous flow mode

Xiang Li [a], Guoqing Zhang [a,*], Huageng Pan [b]

[a] Faculty of Materials and Energy, Guangdong University of Technology, Guangzhou, Guangdong, 510006, China
[b] Shunde Dowell Science & Technology Environmental Protection Engineering Co., Ltd., Shunde, Guangdong, 528300, China

ARTICLE INFO

*Article history:*
Received 26 June 2011
Received in revised form 1 November 2011
Accepted 2 November 2011
Available online 9 November 2011

*Keywords:*
Advanced oxidation technology (AOT)
$H_2S$
Deactivation
Regeneration
$TiO_2$ photocatalyst

ABSTRACT

A foam nickel support was coated with $TiO_2$ sols containing anatase particles. The malodorous compound, hydrogen sulfide ($H_2S$), was removed via photolytic and photocatalytic oxidation processes under ambient conditions using a self-made photoreactor with 185-nm ozone ($O_3$) lamp illumination. The reactor degraded $H_2S$ with high removal efficiency. The effects of several factors, such as initial $H_2S$ concentration, ultraviolet light wavelength, relative humidity (RH), oxygen content, and catalyst deactivation and regeneration, on $H_2S$ degradation were investigated. The highest activity for $H_2S$ destruction was achieved with 80% RH, 21% oxygen content, approximately 200 mg/m$^3$ initial concentration, and 185-nm $O_3$ lamp illumination, resulting in higher conversion. Sulfur ($S^0$) and sulfate ion ($SO_4^{2-}$) were detected as byproducts via the XPS technique. The catalytic activity was improved by $SO_4^{2-}$ promotion, but reduced by $S^0$ accumulation on the photocatalyst surface. In addition, by increasing the amount of $SO_4^{2-}$ generated, the yield of $S^0$ and catalyst poisoning could be controlled in the reaction.

© 2011 Elsevier B.V. All rights reserved.

## 1. Introduction

Malodorous gaseous pollutants in both municipal and industrial waste treatment facilities, as well as in many industrial processes, have become a growing concern because they are a nuisance to the ambient environment and a human health risk. Hydrogen sulfide ($H_2S$) is one of the substances mainly responsible for the offensive odor emitted by wastewater treatment facilities and industrial plants. $H_2S$ is colorless, corrosive, and highly toxic with an extremely low odor threshold [1–3]. $H_2S$ can be produced and released into the atmosphere by many industrial processes. Currently, there are more than 70 occupation types that involve contact with hydrogen sulfide. Among these occupations are those related to mining, leather production, synthetic rubber manufacturing, gas extraction, papermaking, printing and dyeing, sugar manufacturing, sewage treatment, garbage disposal, etc. [4]. In addition, even low $H_2S$ concentrations can severely corrode the metal components of manufacturing facilities. The effective removal of $H_2S$ has thus become a focus of interest. Heterogeneous techniques that mitigate the $H_2S$ contamination problem in external environments include biofiltration, wet scrubbing with chemical solution adsorption, thermal incineration combined with catalytic processes, etc. [5–13]. Although many of these processes have already been applied in manufacturing facilities, these conventional methods have their own limitations. Several mitigation measures are difficult to apply because of safety concerns on the handling of chemicals required for use as scrubbing agents, lack of long-term stability, or high-energy consumption.

Titanium dioxide ($TiO_2$)-mediated photocatalytic reactions have attracted great attention in the air treatment field because of their mild reaction conditions, low cost and energy consumption, and harmless by-products [14]. Indeed, their demand is reflected in the increasing number of publications that deal with both theoretical and practical application aspects of these reactions. The destruction of volatile organic compounds (VOCs) in the gas phase using $TiO_2$/UV has been actively and widely investigated. VOC destruction is performed at room temperature and ambient pressure; thus, additional reagents are not required. The final products show little or no toxicity, compared with the parent compounds. It has been demonstrated that this process can be used to destroy a wide range of VOCs [15–18]. However, the photodestruction of inorganic compounds, including sulfur-containing ones, has yet to be fully explored.

In the research described in the current paper, optimization of the photolytic and photocatalytic destruction of $H_2S$ in the gas-phase is studied. Important parameters affecting the reaction, such as the effects of initial $H_2S$ concentration, ultraviolet light wavelength, relative humidity (RH), oxygen content and photocatalytic deactivation and regeneration, are described. $H_2S$ destruction was

* Corresponding author. Tel.: +86 13632315436; fax: +86 20 39322570.
*E-mail address:* leehyung83@163.com (G. Zhang).

0304-3894/$ – see front matter © 2011 Elsevier B.V. All rights reserved.
doi:10.1016/j.jhazmat.2011.11.006

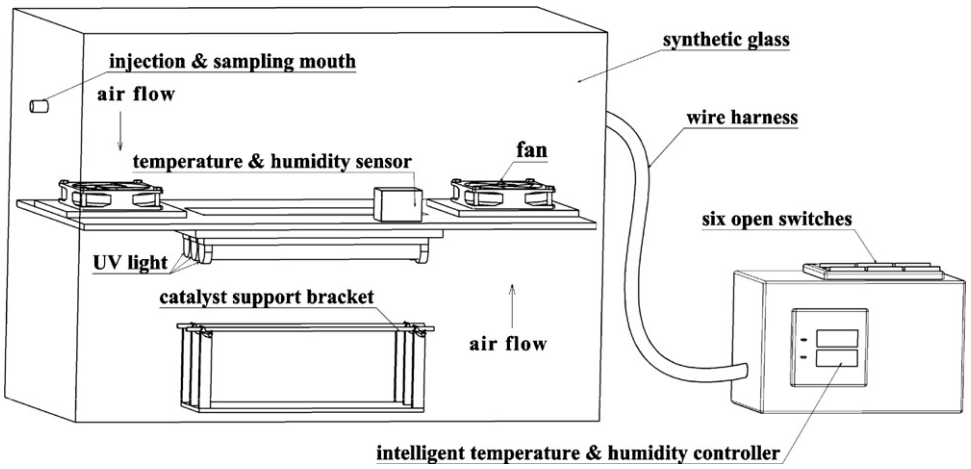


**Fig. 1.** Scheme of the experimental apparatus utilized for $H_2S$ degradation.

performed under laboratory conditions, and the results demonstrated that photolytic and PCO processes can degrade $H_2S$ gas.

## 2. Experimental method

### 2.1. Catalyst support and test methods

#### 2.1.1. Support description

The foam nickel catalyst support (thickness, 3.12 mm; area, 0.113 $m^2$; total weight, 69.056 g; model, 35PPI; voidage, 95%; surface density, $500 \pm 50$ g/$m^2$; $TiO_2$ loading density, 30 g/$m^2$; and grain diameter, 20 nm) was prepared via the sol–gel method. Nano-$TiO_2$ was loaded evenly on the surface of this support. It should be noted that the area of the catalyst support used in each experiment was constant, and its value was 0.113 $m^2$. The area was calculated by multiplying the support length by its width.

#### 2.1.2. $H_2S$ determination

$H_2S$ concentration was determined by the methylene blue spectrophotometric method, which is described in GB/T 11742-1989, "Standard method for hygienic examination of hydrogen sulfide in air of residential areas".

#### 2.1.3. Ozone ($O_3$) determination

$O_3$ concentration was determined by a portable $O_3$ analyzer (GD80, Keernuo Technology Co. Ltd., Shenzhen, China). Prior to the experiment (before the lamps were switched on), the ozone detected in the photoreactor originated from the ozone in the air. Its concentration was about 0.02–0.04 ppm. However, at the beginning of the experiment, this original data was initially set to zero such that the original ozone concentration would not affect the data that was monitored during the experiment. Then, a 60-mm long flexible rubber hose was used to connect the $O_3$ analyzer probe head and the injection and sampling mouth, ensuring a tight seal at the connection points. After approximately 1 min, after obtaining a stable reading, the data displayed on the screen was recorded.

### 2.2. Photodegradation apparatus

The basic experimental setup used in this study is shown in Fig. 1.

The photoreactor, which is an inner gas circulation system, was constructed using 8-mm thick synthetic glass. Silver paper was pasted onto the inner wall of the photoreactor to prevent UV light from leaking during the experiment. The effective volume of the photoreactor was approximately 120 L. Inside the reactor, illumination was provided by three types of 8-W UV lamp (185, 253.7, and 365 nm); these lamps were fixed together at the center of the reactor. The circulatory power of the inner gas was supplied by two small fans with 3.60-W power. These two fans were installed in reverse directions at both sides of the reactor. The average circulation rate of the internal air flowing through the catalyst support surface was measured to be approximately 0.3 m/s using an intelligent anemometer (ZRQF, Beijing Detection Instrument Co. Ltd., Beijing, China). The temperature and humidity inside of the device were monitored by an intelligent temperature and humidity controller (SPD319-WHD, Cai Huang Instrument Technology Co. Ltd., Chongqing, China). All power components were controlled by six open switches.

### 2.3. Experimental methods

$H_2S$ gas was injected using a syringe into the reactor. Both sides of the fan switch were opened more or less simultaneously to ensure that the mixture gas circulating inside the reactor in the absence of UV illumination until gas–solid adsorption equilibrium under the flow was established. The equilibrium state was indicated by identical initial $H_2S$ concentrations. Then, the UV light was switched on to start the experiment, and the $H_2S$ conversion rate was monitored as a function of time by measuring the $H_2S$ concentration during the experiment. A steady state was achieved 70 min after the UV light was switched on. The $H_2S$ concentration in the internal device was measured every 15 min. $H_2S$ conversion was calculated according to Eq. (1):

$$\eta = 1 - \frac{C}{C_0} \times 100\% \quad (1)$$

where $C_0$ is the initial concentration and $C$ is the measured concentration (every 15 min) during the experiment. At the end of the experiment, fresh air was blown into the reactor using an electric fan at maximum speed for more than 2 h to restore initial conditions before running the next experiment. The ventilation in the laboratory was ensured to be adequate. Most experiments were performed at atmospheric pressure, with $30 \pm 5$ °C temperature and $85\% \pm 12\%$ RH conditions.

## 3. Results and discussion

### 3.1. Blank test

A blank test demonstrated the comprehensive effect of $H_2S$ removal with nano-$TiO_2$ loaded on the foam nickel support under

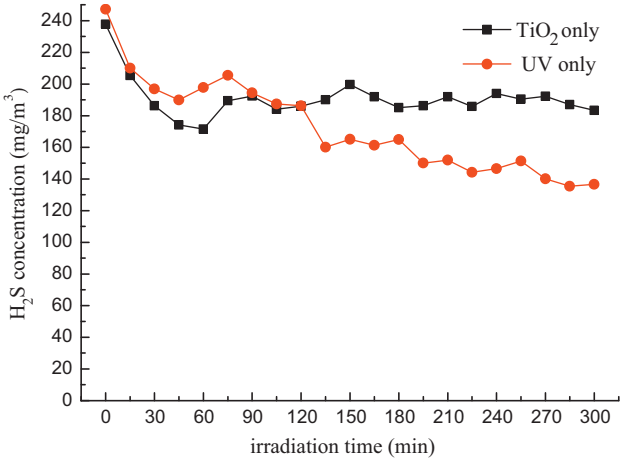


**Fig. 2.** Decomposition of $H_2S$ in the blank test. Experimental conditions: $O_3$ lamp, 185 nm and 8 W; average flow rate, 0.3 m/s; oxygen content, 21%; initial concentrations, 247.27 and 237.76 mg/m$^3$; temperature, 30 ± 2 °C; and relative humidity, 84% ± 3%.

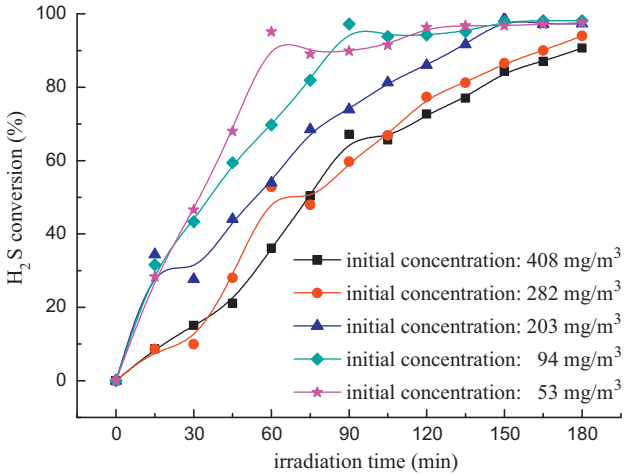


**Fig. 3.** Effects of different initial concentrations on $H_2S$ removal efficiency. Experimental conditions: $O_3$ lamp, 185 nm and 8 W; average flow rate, 0.3 m/s; oxygen content, 21%; temperature, 30.0–31.5 °C; and relative humidity, 78.3–80.1%.

$O_3$ lamp irradiation. Fig. 2 shows that the $H_2S$ concentration in the photoreactor initially decreased and then increased because of the effects of gas diffusion, adsorption, etc. A new adsorption equilibrium was achieved at approximately 70 min after all of the $H_2S$ gas was injected into the reactor. Fig. 2 further shows that after the adsorption equilibrium was reached, there was almost no $H_2S$ degradation in the presence of the $TiO_2$-loaded foam nickel catalyst support (in the absence of UV lamp irradiation). The concentration of $H_2S$ was approximately 190 mg/m$^3$ after the adsorption equilibrium was reached.

The effect of $H_2S$ degradation in the presence of $O_3$ lamp illumination (in the absence of $TiO_2$-loaded foam nickel catalyst support) was obvious. After 300 min of $O_3$ lamp irradiation, the $H_2S$ concentration was reduced by approximately 60–70 mg/m$^3$, and the removal efficiency was approximately 30%. Moreover, in the current process, approximately 8.39 ppm $O_3$ was generated, as measured by the $O_3$ detector (GD80, Keernuo Technology Co. Ltd., Shenzhen, China) under 5 h of $O_3$ lamp irradiation. Many studies have shown that the addition of $O_3$ to photocatalytic processes increases the conversion of contaminants [19–24]. In fact, $O_3$ has been used to capture excited electrons and prevent electron–hole pairs from recombining. $O_3$ forms $O_3^-$, which can directly participate in the reaction [20]. Thus, the role of $O_3$ was deemed important when the effects of the photolytic degradation of $H_2S$ were studied in the current paper; the PCO process greatly contributed to $H_2S$ removal efficiency.

### 3.2. Effects of $H_2S$ initial concentration

The effects of the initial concentration of $H_2S$ on its decomposition are shown in Fig. 3. The results were obtained with temperatures of 30.0–31.5 °C and an RH of 78.3–80.1%. The $H_2S$ concentrations decreased sharply with the extension of $O_3$ lamp irradiation time in the $O_3$/UV/$TiO_2$ process. As shown in Fig. 3, the efficiency of photolytic and photocatalytic $H_2S$ degradation reached the highest levels within the first 90 min after the experiment started. The slope of the curve was steep during this stage in each experiment. After the first 90 min had passed, the $H_2S$ removal efficiency significantly slowed down and the slope of the curve relatively flattened. Therefore, it is necessary to adjust the irradiation time for photolytic and PCO of $H_2S$ in practical engineering applications. Based on Fig. 3, the best range of initial $H_2S$ concentration was determined. When the initial concentration was equal to or less than 200 mg/m$^3$, the highest degradation efficiency with a conversion rate of over 97% was achieved. The default $H_2S$ concentration in the current study was thus set to approximately 200 mg/m$^3$.

### 3.3. Effects of ultraviolet light wavelength

As an essential component to the photolytic and PCO reaction process, the wavelength of UV light has a great effect on $H_2S$ decomposition. Theoretically, UV light with wavelength less than 387.5 nm could activate titania photocatalysts [16]. In the current experiment, three types of 8-W UV lamp (185, 253.7, and 365 nm) were used as UV irradiation sources. The effect of UV light wavelength on $H_2S$ conversion by photolytic and PCO process is shown in Fig. 4. It was found that with the illumination of three types of UV lamp, the conversion of $H_2S$ under 185-nm $O_3$ lamp irradiation was much higher than under 254- and 365-nm irradiation. After a 3-h illumination, 97.4% of $H_2S$ was decomposed when irradiated with the 185-nm UV lamp, whereas only 39.1% and 33.1% $H_2S$ were removed with the irradiation of the 254- and 365-nm UV lamps, respectively. When irradiated by these three types of light, with enough activation energy provided by photons from UV light, electron and hole pairs are generated on the catalyst surface. Moreover,

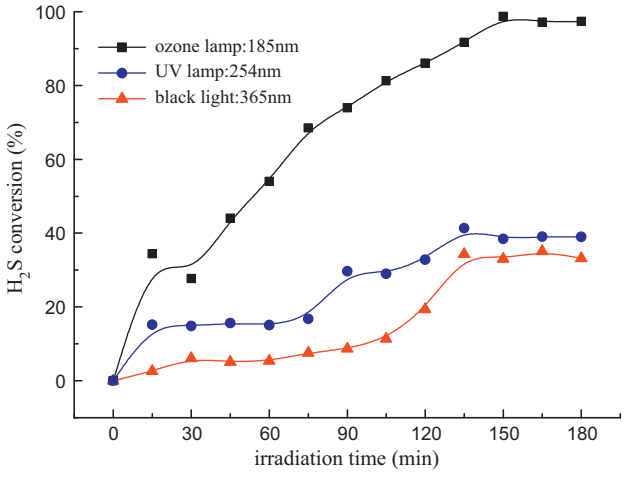


**Fig. 4.** Effects of different wavelengths of UV lamp on $H_2S$ decomposition. Experimental conditions: UV lamp (185, 254, and 365 nm; 8 W); average flow rate, 0.3 m/s; oxygen content, 21%; initial concentrations, 191.83–214.49 mg/m$^3$; temperature, 28.5–31.4 °C; and relative humidity, 77.2–80.9%.

the shorter the wavelength of the UV light, the higher the energy of a single photon. In the case of a constant power of 8 W, the single photon energy provided by the 185-nm light was higher than that provided by the 254- or 365-nm light [19]. These results show that when the photon energy is increased, the $H_2S$ degradation becomes more efficient.

Significant differences in the $H_2S$ removal efficiency resulting from 185-, 254-, and 365-nm UV lamp illumination could also be attributed to another reason. The three UV lamps produced different amounts of $O_3$ during the photolytic and PCO reaction and had different abilities in decomposing $O_3$. In the current experiment, approximately 5.95 ppm $O_3$ was generated under 185-nm lamp illumination in the photoreactor, whereas only 0.32 ppm $O_3$ was generated by the 254-nm lamp; almost no $O_3$ was generated by black light within 3 h of irradiation. As a good electron acceptor, $O_3$ can effectively prevent the recombination of electron–hole pairs and prolong the lifetime of the hole [23]. In addition, $O_3$ adsorbs 185- and 254-nm light and decomposes to form hydroxyl radicals, while 365-nm light cannot efficiently decompose $O_3$ such that almost no reaction occurs between $O_3$ and 365-nm light [19]. The generation of hydroxyl radicals in the $O_3/TiO_2$/UV process is generally described as follows [19,20,23,24]:

$$TiO_2 + h\nu \rightarrow h^+ + e^- \quad (2)$$

$$h^+ + H_2O \rightarrow OH^\bullet + H^+ \quad (3)$$

$$O_3 + e^- \rightarrow O_3^{-\bullet} \quad (4)$$

$$H^+ + O_3^{-\bullet} \rightarrow HO_3^\bullet \quad (5)$$

$$HO_3^\bullet \rightarrow O_2 + OH^\bullet \quad (6)$$

$$O_3 + h\nu(\lambda < 310\,\text{nm}) \rightarrow O^\bullet + O_2 \quad (7)$$

$$O^\bullet + H_2O \rightarrow 2OH^\bullet \quad (8)$$

When irradiated with 185- and 254-nm light, the produced $O_3$ acted as both electron acceptor and hydroxyl radical source. However, when illuminated with 365-nm light, no $O_3$ is produced during the process and the reactions (4)–(8) do not occur. Hence, the $O_3/UV/TiO_2$ process is more efficient than the $UV/TiO_2$ process. Overall, $H_2S$ conversion is highest under the illumination of 185-nm light, and conversion with the 254-nm light is higher than that with the 365-nm one.

### 3.4. The role of water vapor

RH obviously influences the photolytic and PCO process. The water vapor adsorbed onto the photocatalyst combines with the electron–hole ($h^+$) and generates some hydroxyl groups, such as $OH^\bullet$, which, in turn, oxidizes pollutants. The PCO reaction is typically dominated by the generation of the hydroxyl radical, exhibiting higher reaction rates with larger amounts of hydroxyl radicals [25–27]. In the absence of water vapor, the photocatalytic degradation of some pollutants is severely retarded. However, excessive molecular water on the catalyst surface will restrain the conversion rate because the presence of water vapor competes with the contaminant for adsorption sites on the photocatalyst, thus reducing the pollutant removal rate [28]. This phenomenon is called “competitive adsorption” between molecular water and the pollutant.

Considering the wide range of humidity in atmospheric conditions, the effects of humidity in the range of 20–90% on $H_2S$ decomposition in the photolytic and PCO process was investigated. After a 180 min of 185-nm lamp illumination, the conversion rates of 21%, 43%, 62%, 70%, 80% and 90% RH were achieved at 28.37%, 38.07%, 73.14%, 78.53%, 97.36% and 96.95%, respectively. Fig. 5 shows the sharp initial increase in $H_2S$ conversion with the increase

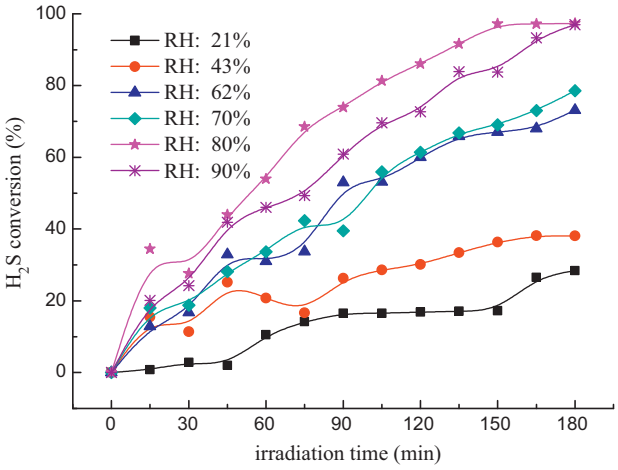


**Fig. 5.** Effects of different relative humidity on $H_2S$ conversion. Experimental conditions: UV lamp, 185 nm and 8 W; initial concentration, 203.31–215.31 mg/m$^3$; average flow rate, 0.3 m/s; oxygen content, 21%; temperature, 30.0–32.8 °C; and relative humidity, 21–90%.

in RH from 21% to 80%. $H_2S$ conversion then slightly decreases at higher humidity, which implies that 80% is the optimal humidity for the photolytic and PCO process. The effect of RH on the decomposition of $H_2S$ is complex. Based on the experiment results, it was noted that the effect of humidity on $H_2S$ decomposition by photolytic and PCO process was two-sided: Increasing humidity improves $H_2S$ decomposition, whereas too much humidity will depress the decomposition. This can be explained by the enhancing effect of humidity on hydroxyl radical generation to decompose more contaminants. At the same time, humidity impedes the contact of $H_2S$ with the $TiO_2$ photocatalyst and $O_3$ to decrease the decomposition.

### 3.5. The role of oxygen

Molecular oxygen is an efficient electron acceptor in the conduction band of the semiconductor, restraining the unpleasant electron ($e^-$)–hole ($h^+$) recombination process. In addition, oxygen is the precursor of various reduced ($O_2^-$, $HO_2^-$, $HO_2^\bullet$, and $H_2O_2$) and very reactive species [29]. Hydroxyl radicals are often considered to be the main charge transfer species contributing to PCO [30]. The presence of oxygen is thus essential for the photolytic and PCO process. The contaminant degradation rate usually increases with increasing oxygen concentration [31], and the competitive adsorption effect between oxygen and the pollutants seems obvious. Therefore, excessive oxygen content will hinder the PCO reaction.

The experiments were performed under conditions of various oxygen contents. The results presented in Fig. 6 shows that at 15% oxygen content, the oxidation rate is at its lowest, reaching just 17.04% after 3 h of illumination. However, when the oxygen content was at 21% (the atmospheric level), $H_2S$ degradation reached the highest conversion rate of 97%. Subsequently, the $H_2S$ removal efficiency sharply decreases at higher oxygen content. The conversion rates of 25% and 30% oxygen contents were achieved at 64.29% and 58.17%, respectively. The results demonstrate that 21% oxygen content is the optimal condition of $H_2S$ degradation in the photolytic and PCO process.

### 3.6. Photocatalyst deactivation and regeneration

A detailed investigation of catalyst deactivation and regeneration was performed under 185-nm light illumination. Each $H_2S$ degradation experiment lasted 5 h using similar internal

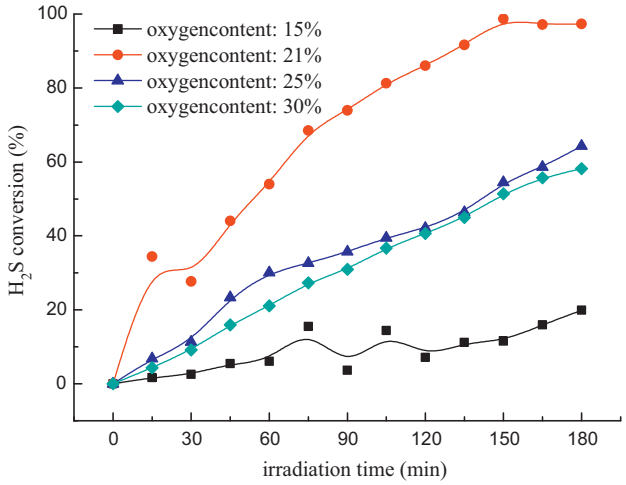


**Fig. 6.** Effects of different oxygen contents on $H_2S$ removal efficiency. Experimental conditions: UV lamp, 185 nm and 8 W; average flow rate, 0.3 m/s; initial concentration, 199.54–245.48 mg/m$^3$; oxygen content (15%, 21%, 25%, and 30%); temperature, 30.1–32.9 °C; and relative humidity, 79.3–85.6%.

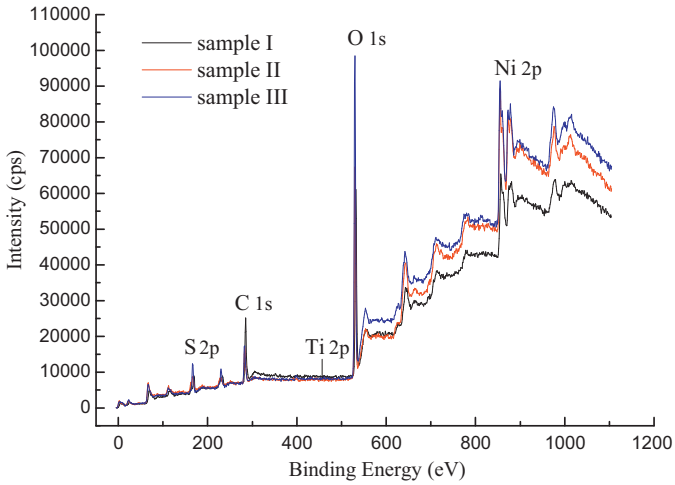


**Fig. 8.** XPS survey spectra of the three $TiO_2$ samples in the different stages of its regeneration (sample I: before regeneration, sample II: regenerated sample, and sample III: sample after 50 h $H_2S$ removal test following regeneration).

concentrations (approximately 200 mg/m$^3$), and the catalyst deactivation was completed within 50 h. Fig. 7 shows that the $H_2S$ degradation yield dropped from 99.60% to 81.58% after 30 h of irradiation. This value dropped even further to 25.88% after 50 h of illumination, which implies that the $TiO_2$ catalyst has ultimately deactivated. After the catalyst deactivation experiment was completed, an electric fan was used for more than 2 h to blow away all the $H_2S$ in the reactor. This allowed fresh air to fill the reactor and ensured that none of the $H_2S$ gas was left. The deactivated catalyst was then irradiated by the 185-nm $O_3$ lamp for 48 h. After this process, the $H_2S$ removal test was again conducted and each test lasted for 5 h under similar previous experimental conditions. During the first 50 h of the $H_2S$ removal process, the average degradation rate remained at 84.21% and the removal rate seemed to increase slightly over time. Therefore, the $TiO_2$ catalyst is successfully regenerated by 48 h of illumination by the 185-nm $O_3$ lamp.

After the first 50 h of $H_2S$ removal experiments, the deactivated $TiO_2$ catalyst was named as sample I (before regeneration) to distinguish it from the regenerated $TiO_2$ sample. Sample I was renamed to sample II (regenerated sample) after it was irradiated by the 185-nm light for 48 h. Sample III was obtained after continuing the $H_2S$ degradation experiments on sample II for 50 h. The three samples were analyzed via XPS (Axis Ultra DLD, Kratos, UK), and the results are shown in the XPS survey spectra and S 2p spectra in Figs. 8 and 9.

Based on the XPS survey spectra (Fig. 8) of the three samples, it was observed that the samples contained Ni, O, Ti, S, C, and other elements. The binding energy was calibrated using the contaminant carbon (C 1s = 284.6 eV) as a reference, then corrected other elements according to the move of the C 1s peak.

The original sample (the $TiO_2$-loaded foam nickel support catalyst prior to any experiment) and samples I, II, and III were analyzed by a scanning electron microscope (S-3400N-II, Hitachi, Japan). The ratios of surface atoms ($S_{total}$) to Ti on the surface of these four samples were 0.310, 25.760, 26.754, and 32.392, respectively. These data show that a small amount of $S^0$ existed in the original sample in the form of impurities, but most of the $S^0$ had been adsorbed onto the surfaces of samples I, II, and III during the $H_2S$ removal experiments. The change in the amount of $S_{total}$ elements between samples I and II was small because none of the $H_2S$ removal experiments were conducted during regeneration. The amount of $S_{total}$ elements in sample III was obviously higher than those in samples I and II because of the additional $H_2S$ removal experiments that were conducted for 50 h after regeneration.

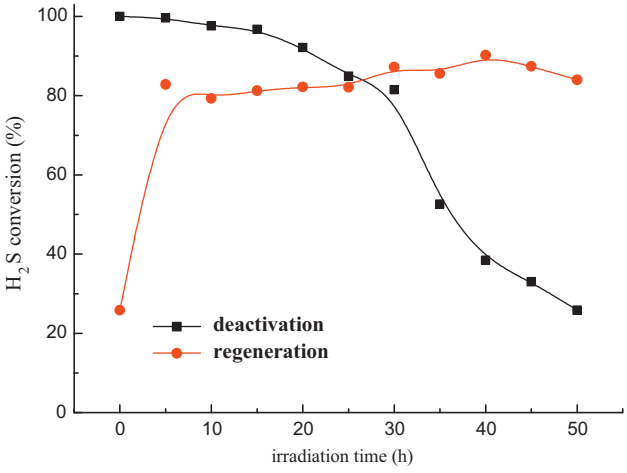


**Fig. 7.** Dependence of $H_2S$ conversion on illumination time. Experimental conditions: UV lamp, 185 nm and 8 W; average flow rate, 0.3 m/s; initial concentration after every 5 h, 211.42–256.17 mg/m$^3$; oxygen content, 21%; temperature, 26.5–28.1 °C; and relative humidity, 77.2% ± 2%.

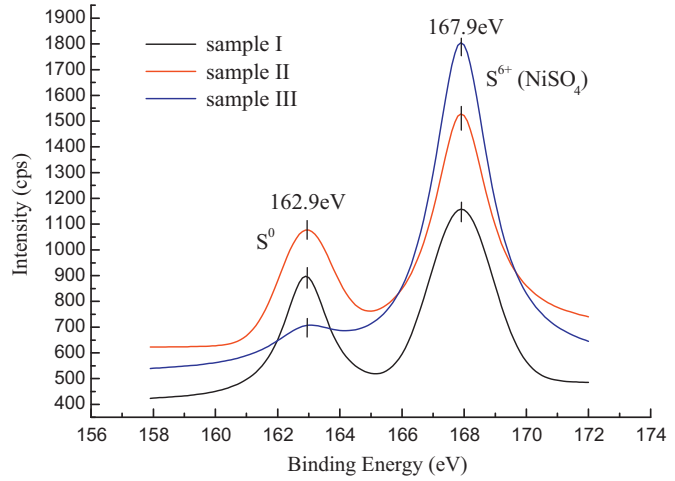


**Fig. 9.** S 2p XPS spectra of the three $TiO_2$ samples in the different stages of its regeneration (sample I: before regeneration, sample II: regenerated sample, sample III: sample after 50 h $H_2S$ removal test following regeneration).

The binding energies of $S^0$ and $NiSO_4$ ($S^{6+}$) are 162.9 and 167.9 eV, respectively. As shown in Fig. 9, the ratios of $S^0$ to $S^{6+}$ on the surfaces of samples I, II, and III were 0.756, 0.314, and 0.122, respectively. During the process from before regeneration to the conduction of 50-h removal experiments after regeneration, the amount of $S^0$ diminished, whereas the amount of $SO_4^{2-}$ increased successively. Moreover, when the catalyst was regenerated, the ratio of $S^0$ to $SO_4^{2-}$ dropped markedly from 0.756 to 0.314, dropping further to 0.122 after the 50-h $H_2S$ degradation experiments were completed. More $S^0$ was contained at the stage before regeneration, but more and more $S^0$ was oxidized into $SO_4^{2-}$ during regeneration. Thus, the photocatalytic activity changed with the different ratios of $S^0$ to $SO_4^{2-}$. The amount of $S^0$ decreased during the additional removal experiments after regeneration, and the average degradation rate reached 84.21%. These results explain the occurrence catalyst poisoning caused by the by-product $S^0$ during the $H_2S$ removal process. Nevertheless, during the additional 50 h removal experiments after regeneration, the formation reaction of $S^0$ was restrained. In addition, the catalyst poisoning was inhibited because of the increase in number of the $SO_4^{2-}$ with $S^0$ reduction on the surface of the catalyst. These results resemble those of other studies on enhancing $TiO_2$ photocatalytic activity by sulfate promotion [32–39]. The $TiO_2$ catalyst can improve catalyst activity by promoting the generation of sulfate. The findings reveal that sulfate modification (super acidification) can not only improve the structure and surface properties of the catalyst, but also boost the PCO activity and stability of the $TiO_2$ catalyst.

Based on the above-mentioned discussion, the mechanisms for $H_2S$ destruction on the photocatalyst surface during the $O_3/UV/TiO_2$ process can be generally proposed as follows [19,20,23,24,29,40]:

$$TiO_2 + h\nu \rightarrow h^+ + e^- \quad (2)$$

$$h^+ + H_2O \rightarrow OH^\bullet + H^+ \quad (3)$$

$$O_3 + e^- \rightarrow O_3^{-\bullet} \quad (4)$$

$$H^+ + O_3^{-\bullet} \rightarrow HO_3^\bullet \quad (5)$$

$$HO_3^\bullet \rightarrow O_2 + OH^\bullet \quad (6)$$

$$O_3 + h\nu(\lambda < 310\,nm) \rightarrow O^\bullet + O_2 \quad (7)$$

$$O^\bullet + H_2O \rightarrow 2OH^\bullet \quad (8)$$

$$h^+ + OH^- \rightarrow OH^\bullet \quad (9)$$

$$O_2 + 2e^- + 2H^+ \rightarrow H_2O_2 \quad (10)$$

$$H_2S + 2OH \xrightarrow{\text{incomplete oxidation}} S\downarrow + 2H_2O \quad (11)$$

$$H_2S + 8OH^\bullet \rightarrow SO_4^{2-} + 2H^+ + 4H_2O \quad (12)$$

$$H_2S + H_2O_2 \xrightarrow{\text{incomplete oxidation}} S\downarrow + 2H_2O \quad (13)$$

$$H_2S + 4H_2O_2 \rightarrow SO_4^{2-} + 2H^+ + 4H_2O \quad (14)$$

## 4. Conclusions

The photolytic and PCO processes decompose $H_2S$ with high removal efficiency under normal experimental conditions. On the basis of this study, the following conclusions could be drawn. The highest activity is reached with 80% RH, 21% oxygen content, and approximately 200 mg/m$^3$ initial concentration under 185-nm $O_3$ light illumination. $H_2S$ degradation initially increases with increasing RH, oxygen content, and initial concentration up to peak point of conversion, and then decreases because of "competitive adsorption" among excessive molecular water, $O_2$, and other pollutants. The $TiO_2$/UV process is much more efficient with the 185-nm lamp than with the 254- or 365-nm lamp.

The XPS results show that the catalyst activity changes with the different ratios of $S^0$ to $S^{6+}$ ($SO_4^{2-}$) on the catalyst surface. The catalyst deactivates when the ratio of $S^0$ to $SO_4^{2-}$ increases. However, this ratio continuously drops during the continuous process of regeneration. With increasing amounts of $SO_4^{2-}$ generated in the reaction, the yield of $S^0$ (catalyst poisoning) could be inhibited.

## Acknowledgements

This work was financially supported by the Science & Technology Plan Project of Guangdong Province (Grant No. 2009B030500001) and the Cooperation Project of Foshan City and Chinese Academy of Sciences (Grant No. 2010YS015). The authors would like to acknowledge Prof. Yongjun Hu and Prof. Xiaoling Cheng for their help during the XPS analysis.

## References

[1] T. Godish, Air Quality, third ed., CRC/Lewis Publishers, Boca Raton, 1997.
[2] J.M.M. De Zwart, J.G. Kuenen, C1-cycle of sulfur compounds, Biodegradation 3 (1992) 37–59.
[3] B. Mills, Review of methods of odour control, Filtr. Sep. 32 (1995) 147–152.
[4] E. Smet, P. Lens, H. Van Langenhove, Treatment of waste gases contaminated with odorous sulfur compounds, Crit. Rev. Environ. Sci. Technol. 28 (1998) 89–117.
[5] X. Jiang, J.H. Tay, Removal mechanisms of $H_2S$ using exhausted carbon in biofiltration, J. Hazard. Mater. 185 (2011) 1543–1549.
[6] D. Ramirez-Saenz, P.B. Zarate-Segura, C. Guerrero-Barajas, E.I. Garcia-Pena, $H_2S$ and volatile fatty acids elimination by biofiltration: clean-up process for biogas potential use, J. Hazard. Mater. 163 (2009) 1272–1281.
[7] S.J. Park, S.I. Nam, E.S. Choi, Removal of odor emitted from composting facilities using a porous ceramic biofilter, Water Sci. Technol. 44 (2001) 301–308.
[8] P. Hardy, J.E. Burgess, S. Morton, R.M. Stuetz, Simultaneous activated sludge wastewater treatment and odour control, Water Sci. Technol. 44 (2001) 189–196.
[9] J. Mitome, G. Karakas, K.A. Bryan, U.S. Ozkan, Effect of $H_2O$ and $SO_2$ on the activity of $Pd/TiO_2$ catalysts in catalytic reduction of NO with methane in the presence of oxygen, Catal. Today 42 (1998) 3–11.
[10] M.Y. Shin, D.W. Park, J.S. Chung, Vanadium-containing catalysts for the selective oxidation of $H_2S$ to elemental sulfur in the presence of excess water, Catal. Today 63 (2000) 405–411.
[11] D.W. Park, S.W. Chun, J.Y. Jang, H.S. Kim, H.C. Woo, J.S. Chung, Selective removal of $H_2S$ from coke oven gas, Catal. Today 44 (1998) 73–79.
[12] J.S. Chung, S.C. Paik, H.S. Kim, D.S. Lee, I.S. Nam, Removal of $H_2S$ and/or $SO_2$ by catalytic conversion technologies, Catal. Today 35 (1997) 37–43.
[13] Y.X. Chen, Y. Jiang, W.Z. Li, R.C. Jin, S.Z. Tang, W.B. Hu, Adsorption and interaction of $H_2S/SO_2$ on $TiO_2$, Catal. Today 50 (1999) 39–47.
[14] S.L.H. Andrew Mills, An overview of semiconductor photocatalysis, J. Photochem. Photobiol. A 108 (1997) 1–35.
[15] Q.L. Yu, H.J.H. Brouwers, Indoor air purification using heterogeneous photocatalytic oxidation. Part I. Experimental study, Appl. Catal. B: Environ. 92 (2009) 454–461.
[16] J.H. Mo, Y.P. Zhang, Q.J. Xu, J.J. Lamson, R.Y. Zhao, Photocatalytic purification of volatile organic compounds in indoor air: a literature review, Atmos. Environ. 43 (2009) 2229–2246.
[17] H.L. Yu, K.L. Zhang, C. Rossi, Theoretical study on photocatalytic oxidation of VOCs using nano-$TiO_2$ photocatalyst, J. Photochem. Photobiol. A 188 (2007) 65–73.
[18] D. Chatterjee, S. Dasgupta, Visible light induced photocatalytic degradation of organic pollutants, J. Photochem. Photobiol. C: Photochem. Rev. 6 (2005) 186–205.
[19] Z. Pengyi, Y.L.F. Gang, C. Qing, Z. Wanpeng, A comparative study on decomposition of gaseous toluene by $O_3$/UV, $TiO_2$/UV and $O_3/TiO_2$/UV, J. Photochem. Photobiol. A 156 (2003) 189–194.
[20] H. Qi, D. Sun, G. Chi, Formaldehyde degradation by UV/$TiO_2/O_3$ process using continuous flow mode, J. Environ. Sci. 19 (2007) 1136–1140.
[21] W. Han, P. Zhang, W. Zhu, J. Yin, L. Li, Photocatalysis of *p*-chlorobenzoic acid in aqueous solution under irradiation of 254 nm and 185 nm UV light, Water Res. 38 (2004) 4197–4203.
[22] C. Guillard, Photocatalytic degradation of butanoic acid Influence of its ionisation state on the degradation pathway: comparison with $O_3$/UV process, J. Photochem. Photobiol. A 135 (2000) 65–75.
[23] L.Y. Sun, H. Lu, J. Zhou, Degradation of H-acid by combined photocatalysis and ozonation Processes, Dyes Pigm. 76 (2008) 604–609.
[24] H.B. Huang, W.B. Li, Destruction of toluene by ozone-enhanced photocatalysis: performance and mechanism, Appl. Catal. B 102 (2011) 449–453.
[25] T.N. Obee, R.T. Brown, $TiO_2$ photocatalysis for indoor air applications: effects of humidity and trace contaminant levels on the oxidation rates of formaldehyde, toluene, and 1,3-butadiene, Environ. Sci. Technol. 29 (1995) 1223–1231.

[26] Y. Luo, D.F. Ollis, Heterogeneous photocatalytic oxidation of trichloroethylene and toluene mixtures in air: kinetic promotion and inhibition, time-dependent catalyst activity, J. Catal. 163 (1996) 1–11.
[27] D.R. Park, J.L. Zhang, K. Ikeue, H. Yamashita, M. Anpo, Photocatalytic oxidation of ethylene to $CO_2$ and $H_2O$ on ultrafine powdered $TiO_2$ photocatalysts in the presence of $O_2$ and $H_2O$, J. Catal. 185 (1999) 114–119.
[28] T.N. Obee, S.O. Hay, Effects of moisture and temperature on the photooxidation of ethylene on titania, Environ. Sci. Technol. 31 (1997) 2034–2038.
[29] C. Maria, R.M.A. Canela, W.F. Jardim, Gas-phase destruction of $H_2S$ using $TiO_2$/UV-VIS, J. Photochem. Photobiol. A 112 (1998) 73–80.
[30] H. Gerischer, A. Heller, The role of oxygen in photooxidation of organic molecules on semiconductor particles, J. Phys. Chem. 95 (1991) 5261–5267.
[31] C.P. Chang, J.N. Chen, M.C. Lu, Heterogeneous photocatalytic oxidation of acetone for air purification by near UV-irradiated titanium dioxide, J. Environ. Sci. Health Part A: Toxic Hazard. Subst. Environ. Eng. 38 (2003) 1131–1143.
[32] G. Colon, M.C. Hidalgo, M. Macias, J.A. Navio, Enhancement of $TiO_2$/C photocatalytic activity by sulfate promotion, Appl. Catal. A 259 (2004) 235–243.
[33] J. Sohn, S.H. Lee, Acidic properties of nickel sulfate supported on $TiO_2$-$ZrO_2$ and catalytic activity for acid catalysis, Appl. Catal. A 266 (2004) 89–97.
[34] X. Wang, J.C. Yu, P. Liu, X. Wang, W. Su, X. Fu, Probing of photocatalytic surface sites on $SO_4^{2-}$/$TiO_2$ solid acids by in situ FT-IR spectroscopy and pyridine adsorption, J. Photochem. Photobiol. A 179 (2006) 339–347.
[35] M.C. Hidalgo, M. Maicu, J.A. Navío, G. Colón, Study of the synergic effect of sulfate pre-treatment and latinisation on the highly improved photocatalytic activity of $TiO_2$, Appl. Catal. B 81 (2008) 49–55.
[36] P. Ciambelli, M.E. Fortuna, D. Sannino, A. Baldacci, The influence of sulfate on the catalytic properties of $V_2O_5$-$TiO_2$ and $WO_3$-$TiO_2$ in the reduction of nitric oxide with ammonia, Catal. Today 29 (1996) 161–164.
[37] B.M. Reddy, P.M. Sreekanth, Yusuke Yamada, Q. Xu, T. Kobayashi, Surface characterization of sulfate, molybdate, and tungstate promoted $TiO_2$-$ZrO_2$ solid acid catalysts by XPS and other techniques, Appl. Catal. A: Gen. 228 (2002) 269–278.
[38] S.Y. Lai, W. Pan, C.F. Ng, Catalytic hydrolysis of dichlorodifluoromethane (CFC-12) on unpromoted and sulfate promoted $TiO_2$-$ZrO_2$ mixed oxide catalysts, Appl. Catal. B 24 (2000) 207–217.
[39] D.S. Muggli, L. Ding, Photocatalytic performance of sulfated $TiO_2$ and Degussa P-25 $TiO_2$ during oxidation of organics, Appl. Catal. B 32 (2001) 181–194.
[40] R. Portela, S. Suárez, S.B. Rasmussen, N. Arconada, Y. Castro, A. Durán, P. Ávila, J.M. Coronado, B. Sánchez, Photocatalytic-based strategies for $H_2S$ elimination, Catal. Today 151 (2010) 64–70.